REPORT DOCUMENTATION PAGE

Form Approved
OMB No. 0704-0188

1. REPORT DATE *(DD-MM-YYYY)*	**2. REPORT TYPE**	**3. DATES COVERED** *(From - To)*
April 2013	Technical Paper	April 2013-July 2013

4. TITLE AND SUBTITLE
Iodine Plasma Species Measurements in a Hall Effect Thruster Plume

5a. CONTRACT NUMBER
FA9300-10-C-2108

5b. GRANT NUMBER

5c. PROGRAM ELEMENT NUMBER

6. AUTHOR(S)
Szabo, J., Robin, R.

5d. PROJECT NUMBER

5e. TASK NUMBER

5f. WORK UNIT NUMBER
Q09A

7. PERFORMING ORGANIZATION NAME(S) AND ADDRESS(ES)

Air Force Research Laboratory (AFMC)
AFRL/RQRS
1 Ara Drive.
Edwards AFB CA 93524-7013

8. PERFORMING ORGANIZATION REPORT NO.

9. SPONSORING / MONITORING AGENCY NAME(S) AND ADDRESS(ES)
Air Force Research Laboratory (AFMC)
AFRL/RQR
5 Pollux Drive
Edwards AFB CA 93524-7048

10. SPONSOR/MONITOR'S ACRONYM(S)

11. SPONSOR/MONITOR'S REPORT NUMBER(S)
AFRL-RQ-ED-TP-2013-052

12. DISTRIBUTION / AVAILABILITY STATEMENT
Distribution A: Approved for Public Release; Distribution Unlimited. PA#13200

13. SUPPLEMENTARY NOTES
Conference paper for the 49th AIAA Joint Propulsion Conference, San Jose, CA, 14-17 July 2013.

14. ABSTRACT

The plasma plume from a 200 W Hall Effect Thruster fueled by iodine vapor was analyzed. The plasma source included a laboratory propellant feed system and a laboratory model Hall thruster powered by a breadboard power processing unit. The hollow cathode was fed with xenon. The distribution of iodine ions was measured with an ExB probe, an electrostatic analyzer (ESA), and a combined ESA/ExB probe. The distribution of xenon ions was also measured. Multiply charge species were detected with both iodine and xenon. Significant populations of diatomic iodine ions were also detected. The dimer fraction was found to vary with operating conditions and angular distance from the beam centroid. The greatest populations of high energy dimers were observed at lower discharge current, and at angles of 30-50 degrees from the beam centroid. At one operating condition, the high energy dimer fraction was approximately 20% by mass in this region. Significant dimer fractions could increase thrust to power by useful amounts at the cost of some overall efficiency.

15. SUBJECT TERMS

16. SECURITY CLASSIFICATION OF:			**17. LIMITATION OF ABSTRACT**	**18. NUMBER OF PAGES**	**19a. NAME OF RESPONSIBLE PERSON**
					Daniel Brown
a. REPORT	**b. ABSTRACT**	**c. THIS PAGE**			**19b. TELEPHONE NO** *(include area code)*
Unclassified	**Unclassified**	**Unclassified**	SAR	20	661-525-5028

Standard Form 298 (Rev. 8-98)
Prescribed by ANSI Std. 239.18

Iodine Plasma Species Measurements in a Hall Effect Thruster Plume

James Szabo[1], Mike Robin[2]
Busek Co. Inc, Natick, MA, 01760, USA

The plasma plume from a 200 W Hall Effect Thruster fueled by iodine vapor was analyzed. The plasma source included a laboratory propellant feed system and a laboratory model Hall thruster powered by a breadboard power processing unit. The hollow cathode was fed with xenon. The distribution of iodine ions was measured with an ExB probe, an electrostatic analyzer (ESA), and a combined ESA/ExB probe. The distribution of xenon ions was also measured. Multiply charge species were detected with both iodine and xenon. Significant populations of diatomic iodine ions were also detected. The dimer fraction was found to vary with operating conditions and angular distance from the beam centroid. The greatest populations of high energy dimers were observed at lower discharge current, and at angles of 30-50 degrees from the beam centroid. At one operating condition, the high energy dimer fraction was approximately 20% by mass in this region. Significant dimer fractions could increase thrust to power by useful amounts at the cost of some overall efficiency.

Nomenclature

$\vec{B}$	=	magnetic field
$\vec{E}$	=	electric field
e	=	charge of an electron, 1.6 x 10^{-19} C
F_t	=	beam momentum in axial direction
f	=	species fraction
g_0	=	gravitational constant at Earth's surface, 9.81 m/s^2
I	=	current, subscripts b for beam, c for cathode, d for discharge, m for magnet
I_{sp}	=	specific impulse
j	=	current density
K	=	mass flow rate divided by discharge current
L	=	characteristic distance/dimension
$\dot{m}$	=	mass flow rate, subscripts a for anode, c for cathode, i for beam ions
M	=	ion mass
P_d	=	discharge power
p	=	pressure, subscript s for sensor, x for xenon
q	=	ion charge
r	=	radial direction or distance
T	=	thrust
t	=	time
V_d	=	discharge potential
v	=	velocity
Z	=	mean ion charge
z	=	axial direction or distance
η	=	efficiency
Γ	=	flux
μ	=	viscosity

[1] Chief Scientist for Hall Thrusters, AIAA Associate Fellow
[2] Research Engineer, AIAA Member

I. Introduction

THE Hall Effect Thruster (HET) is an efficient form of electric propulsion that is typically used in space for orbit-raising and orbit maintenance. Hall thrusters were invented in the United States, but first transitioned to flight in the Soviet Union. [1, 2, 3, 4] The first American HET to fly in space was the Busek BHT-200, launched in 2006 as part of the US Air Force TacSat-2 satellite and fueled by xenon.[5] Testing of a BHT-200 fueled by iodine vapor yielded stability and performance comparable to that observed with xenon.[6] Plume current measurements with the same thruster showed lower beam divergence and the presence of I_2^+ near the beam centroid.[7] Testing of a 1-kW thruster fueled by iodine also showed high efficiency and low beam divergence.[8]

This paper report iodine ion energy and species distributions measurements carried out with an experimental version of the BHT-200 shown in . These measurements were obtained with an ExB probe, an electrostatic analyzer (ESA), and a combined ESA/ExB probe at various operating conditions and angles with respect to the beam centroid. The paper also provides a discussion of how the composition of the iodine plume may affect efficiency and thrust to power.

A. Hall Thruster Physics

A Hall effect thruster uses crossed electric and magnetic fields to generate and accelerate ions. The gas in the discharge is partially ionized, although propellant utilization may approach 100%. The overall structure of the BHT-200 is defined by a magnetic circuit that produces a steady magnetic field, $\vec{B}$, in the nominal radial direction across an annular channel.[9] Neutral propellant is introduced through the anode at the base of the channel. The downstream portion of the channel is formed by a dielectric material, between which the bulk of the plasma discharge occurs. A potential difference, V_d, is applied between the anode and a hollow cathode located outside the channel. The resulting electric field, $\vec{E}$, is predominantly axial and is concentrated near the channel exit by interactions between the magnetic field and the plasma. Typically the cathode is allowed to float with respect to facility ground.

Fig. 1 Iodine Thruster in Test Facility

In the channel, electrons are strongly magnetized and their transport is predominantly azimuthal due to the $\vec{E}\times\vec{B}$ Hall Effect. The extended electron path enables an efficient, impact driven ionization cascade. The peak electron temperature is typically several tens of volts. Axial transport across $\vec{B}$ is provided by collisions, wall effects, and additional, "anomalous" transport identified in the early 1960s.[10] Ions are weakly magnetized and most are accelerated directly out of the channel, forming the ion beam. The bulk of the cathode electrons go to neutralize the ion beam current, I_b. However, some circulate back through the channel, driven by the potential difference. These electrons seed the discharge cascade. A control volume analysis shows that the discharge current, I_d, is equal to the cathode current, I_c, which is equal to the sum of I_b and the electron flux to the discharge.

B. Rationale for Iodine

Iodine propellant may be used in Hall thrusters, ion engines, and other types of plasma based thrusters. Table 1 compares some key properties of iodine with those of the noble gas xenon. Atomic iodine is lighter than xenon, but iodine stores and vaporizes as a diatomic molecule, I_2. Furthermore, ionization energies and electron impact ionization cross sections for I and I_2 are larger than ionization energies and cross sections for Xe.[14,11] These attributes make iodine easier to ionize than xenon, which result in similar or greater propellant utilization. Iodine performance measurements indicate little or no efficiency penalty with respect to xenon.[6,8] At equivalent operating points, thrust to power sometimes increases, but this is typically counterbalanced by lower specific impulse. Measurements also show consistently lower beam divergence with iodine.

Table 1 Properties of iodine and xenon.[12, 13, 14.]

Element	I	Xe
Atomic Mass	126.9	131.3
Ionization Properties (monatomic)		
First Ionization Potential (eV)	10.5	12.1
Peak Cross Section (10^{-16} cm^2)	6.0	4.8
Storage and Handling Properties		
Storage density (gm/cm^3) near room temp.	4.9	1.6*
Melting Point (^oC)	113.7	-112
Boiling Point at 10 Pa (^oC)	9	-181
*14 Mpa, 50 C (NIST Database)		

Storage and handling properties for iodine and xenon are very different. Iodine stores in the solid phase at approximately three times the density of xenon. The vapor pressure required to fuel a thruster (much less than 1 atmosphere), may be generated by heating the solid to a modest temperature, e.g. 80 - 100 degrees C. Xenon must be stored in h high pressure tanks or at cryogenic conditions.

The only significant disadvantage to iodine is that it is a halogen, which means it is reactive with some substances. However, the vapor pressure of I_2 is greater than 1 Pa at -12 C, which suggests minimal deposition on spacecraft surfaces. Furthermore, inside the thruster, condensation will not occur at typical operating temperatures. Reactivity with wetted surfaces is an issue, but this may be addressed though material selection.

C. Unique Features of the Iodine Discharge

In a typical Hall thruster, ionization is produced through inelastic scattering of high energy electrons off a neutral gas that is flowing through the channel. The electron impact ionization reactions for iodine are as follows:

$$e + I \rightarrow 2e + I^+ \quad (1a)$$

$$e + I \rightarrow 3e + I^{2+} \quad (1b)$$

$$e + I_2 \rightarrow 2e + I_2^+ \quad (1c)$$

$$e + I_2 \rightarrow 3e + I_2^{2+} \quad (1d)$$

Fig. 2 shows electron impact ionization cross sections for these reactions.[15] The ionization energies for I and I_2 are 10.5 and 9.3 eV, respectively.

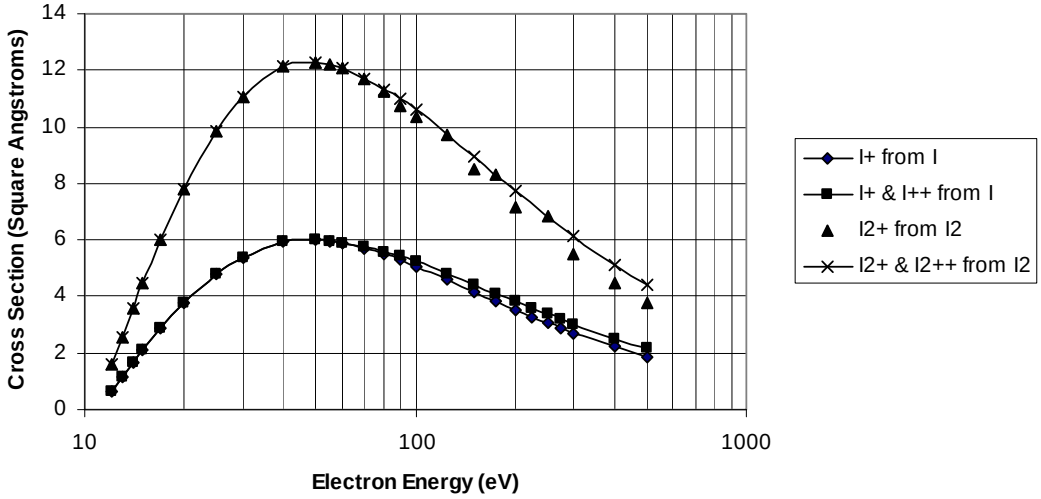

Fig. 2 Iodine ionization cross sections

Dissociation is also caused by inelastic scattering:

$$e + I_2 \rightarrow e + I + I\,. \tag{2a}$$

Although the I_2 dissociation energy of 1.57 eV[12] is far lower than the electron temperature in the discharge, the measured presence of I_2^+ in the plume suggests dissociation is incomplete. Dissociation processes may also produce ions through the reactions

$$e + I_2 \rightarrow 2e + I + I^+ \tag{2b}$$

and

$$e + I_2 \rightarrow 3e + I^+ + I^+\,. \tag{2c}$$

Dissociative ionization obviously requires more energy than mere dissociation, but electron temperatures of ~20 eV are predicted in the channel of a xenon fueled BHT-200 by the hybrid Particle-in-Cell modeling code HPHall. [16, 17]

Negative ions may also be present in the iodine discharge. These are formed through attachment processes. If formed, negative ions would move upstream toward the anode, where they would most likely be recycled

Charge exchange collisions are also present. These are particularly important in the ion beam, where the particles have long distances to interact. Some reactions include

$$I + I^+ \rightarrow I^+ + I\,, \tag{3a}$$

$$I + I_2^+ \rightarrow I^+ + I_2\,, \tag{3b}$$

$$I + I^{2+} \rightarrow I^+ + I^+\,, \tag{3c}$$

$$I_2 + I^+ \rightarrow I_2^+ + I\,, \tag{3d}$$

$$I_2 + I_2^+ \rightarrow I_2^+ + I_2\,, \tag{3e}$$

and

$$I_2 + I^{2+} \rightarrow I_2^+ + I^+\,. \tag{3f}$$

All of the listed ionic species are measured in the plume.

Over long distances, ion recombination could significantly diminish the dimer population and affect interpretation of plume measurements. However, recombination is likely to be minimal, and in modeling xenon Hall thrusters,[18] it is often ignored.

In prior work, the composition of the flight model BHT-200 thruster plume was measured with an ExB probe located near the beam centroid at one operating condition ($V_d = 250$ V, $P_d \sim 200$ W). The primary iodine ionic species in the plume are I^+, I^{2+}, and I_2^+. Per Table 2, approximately 3% of the iodine plume was found to consist of diatomic ions. This was twice the size of the measured I^{2+} fraction and 40% larger than the Xe^{2+} fraction.[6,7] However, variations in space and with operating conditions were not explored. The degree of dissociation may not be uniform throughout the discharge and plume, or constant with respect to plasma density and electron temperature, which vary with I_d and V_d.

Table 2 Iodine molar flux fractions at 250 V and ~200 W

Species	Mole Fraction (%)
I^+	95.3
I_2^+	2.9
I^{2+}	1.5
I^{3+}	0.3

D. Kinetic View of the Beam

The beam ion current is the sum of k ionic species:

$$I_b = \sum_k I_k = \sum_k \dot{m}_k \frac{q_k}{M_k}. \tag{4}$$

Here, q is the ion charge, M is the ion mass, and $\dot{m}$ is the total species mass flow rate. Thrust is determined by the axial (Z-direction) momentum carried by the heavy particles

$$F = \sum_k \dot{m}_k < v_{k,z} >. \tag{5}$$

Most momentum is carried by the ionic species, although modeling and testing of xenon thrusters shows a small but measurable fraction of the momentum is carried by neutrals. The momentum carried by an individual ion at energy ε is given by $p = Mv$, where

$$v = \sqrt{\frac{2qV}{M}} = \sqrt{\frac{2\varepsilon}{M}}\,. \tag{6}$$

Here, V is the potential through which the ion has been accelerated, given by $V = V_d - \sum_i \Delta V_i$. The loss term accounts for the floating cathode potential and the point of ion origin with respect to the anode potential.

The mean exhaust velocity or specific impulse is defined by thrust, $I_{sp} = F / \dot{m} g_0$. Here, $\dot{m}$ is the total thruster mass flow rate, and g_0 is the force of gravity at the surface of the Earth. The ratio of thrust to power (F / P) available at a particular I_{sp} determines the efficiency:

$$\eta = \frac{F}{P}\frac{I_{sp} g_0}{2} = \frac{F^2}{2\dot{m}P}\,. \tag{7}$$

The relationship between F / P and I_{sp} is plotted for thruster efficiencies between 50% and 100%. The only way to increase F / P at constant I_{sp} is to increase efficiency.

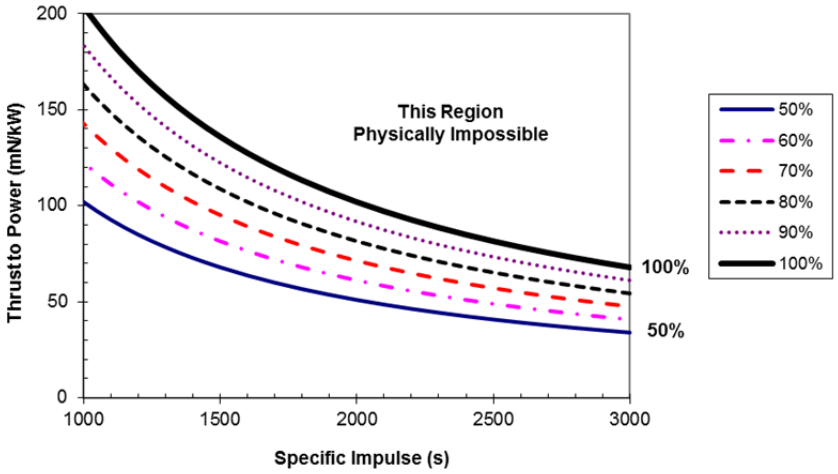

Fig. 3 Relationship Between Thrust to Power and Specific Impulse

For thruster analysis, often only the anode propellant flow rate and discharge power are considered when formulating the efficiency. This anode or thrust efficiency may be expressed as the product of the propellant utilization efficiency (η_u), electrical efficiency (η_e), acceleration efficiency (η_a) and beam efficiency, (η_b),

$$\eta_t = \eta_u \eta_e \eta_a \eta_b\,. \tag{8}$$

The propellant utilization efficiency is the ratio of the beam ion mass flow rate to the anode mass flow rate; $\eta_u = \dot{m}_i / \dot{m}_a$. The electrical efficiency is the ratio of ion beam current to discharge current, $\eta_e = I_b / I_d$. The acceleration efficiency is the ratio of the total potential through which the ions are accelerated to the discharge potential; $\eta_a = (V / V_d)$. Following the method of Ref. 19, the beam efficiency may be expressed as $\eta_b = \eta_s F_t^2$. The thrust correction factor, F_t, accounts for momentum lost to beam divergence. The species efficiency, η_s,

accounts for the momentum spread in a beam with particles of multiple sizes. When analyzing colloidal thrusters, Lozano called this concept polydispersivity. [20] This concept was referred to as propellant efficiency by Brown et al.[21]

If the thruster efflux is assumed to be symmetric about the beam centroid, the number of particles crossing a hemispherical surface distance *r* from the thruster exit is given by

$$\frac{dN}{dt} = 2\pi r^2 \int_0^{\pi/2} \Gamma(\theta)\sin(\theta)d\theta . \tag{9}$$

Here, θ is measured from the plume centroid, and $\Gamma(\theta) = n < v_r >$ is the local flux in the radial direction. Integrating the ion current density, $j(\theta)$, over the surface gives the beam current;

$$I_b = 2\pi r^2 \int_0^{\pi/2} j(\theta)\sin(\theta)d\theta . \tag{10}$$

By species, the molar (number) fraction of $\Gamma(\theta)$ crossing the surface is given by h_k, where $\sum_k h_k = 1$. Thus, ion current by species is proportional to $\sum_k h_k q_k$ and mass flux by species is proportional to $\sum_k h_k M_k$. Here, the normalized current and mass flux fractions are called f_k and g_k, respectively.

The thrust, which is equivalent to the change in axial momentum per unit time, is given by

$$F = \frac{dp_z}{dt} = 2\pi r^2 \int_0^{\pi/2} \Gamma M v_r \cos(\theta)\sin(\theta)d\theta . \tag{11}$$

If the momentum flux, $\Gamma M v_r$, is assumed to vary in proportion to $j(\theta)$, then the fraction of the beam momentum that is in the axial direction may be estimated through the relation

$$F_t = \frac{2\pi r^2 \int_0^{\pi/2} j(\theta)\sin(\theta)\cos(\theta)d\theta}{I_b} . \tag{12}$$

This relationship essentially assumes that average ion speed, charge, and mass are constant with angle. However, as reported in this paper, h_k, f_k and g_k may vary across the plume. Furthermore, ion energy measurements here and historically show non-Maxwellian ion velocity distributions that vary with proximity to the beam centroid and thruster exit.[28]

The degree to which the local composition of the plume affects thruster performance may still be gauged by $j(\theta)$, which decreases with θ at a roughly exponential rate. However, on doing so, the weighting factors of equations 9-12 must be considered. The flux and beam current weighting factor, $\sin(\theta)$, peaks at 90 degrees, while the thrust weighting factor, $\sin(\theta)\cos(\theta)$, peaks at 45 degrees. This counteracts, to some extent, the exponential decay of the plume and it makes the composition of the beam out to at least 45 degrees significant with regard to performance. The weighting functions are plotted in Fig. 4.

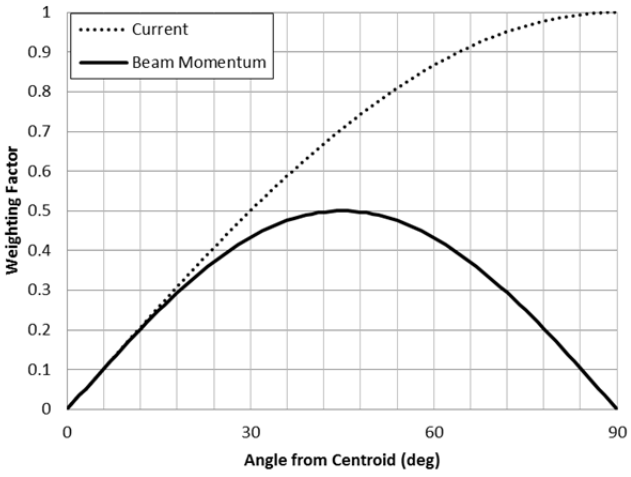

Fig. 4 Weighting factors as a function of angle

II. Apparatus and Procedure

In this research, the plume of a low power laboratory model iodine fueled Hall thruster was measured with electrostatic and electromagnetic plasma wetted probes.

A. Hall Thruster System

The Hall thruster used for this research was an experimental version of the Busek BHT-200. The beam was neutralized by a barium impregnated hollow cathode flowing xenon. The system was powered by a breadboard power processing unit (PPU). Operationally, the thruster was pre-heated with a xenon discharge before switching over to iodine. Fig. 5 shows the iodine plume during testing.

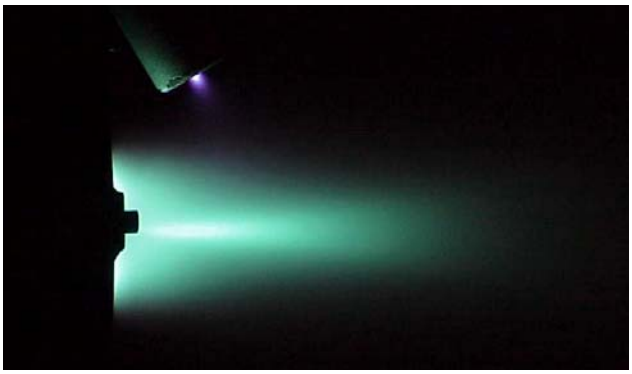

Fig. 5 Iodine Plume from 200 V Discharge

B. Xenon Feed System

Xenon flow was regulated by Unit 7300 series flow controllers sourced from Unit Instruments. The anode was fed with a 50 SCCM controller, which was calibrated to minimize uncertainty at flow rates of interest. The cathode was fed with a 10 SCCM controller.

C. Iodine Feed System

I_2 was sublimed from high purity crystals inside a thermally controlled reservoir located outside the vacuum tank. The I_2 vapor passed through a heated line to the thruster located under vacuum. The flow rate was controlled by regulating the temperature (hence pressure) at the source as described in Ref. 6. The system is shown in Fig. 6.

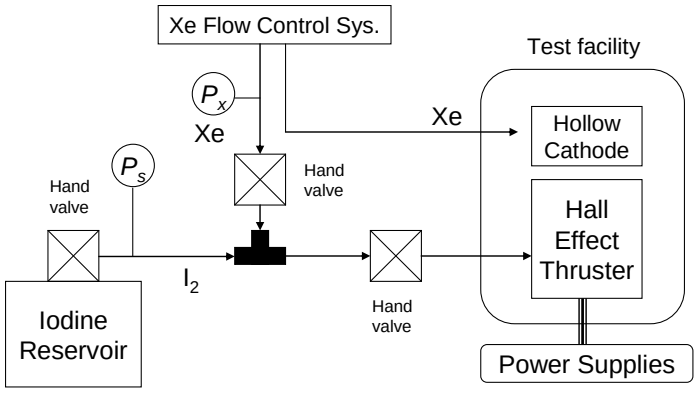

Fig. 6 Iodine Feed System.

D. Test Facility

The system was tested in Busek's 1.8 meter diameter, 3.7 meter long T6 vacuum facility. The facility is equipped with a 32 inch diameter diffusion pump with an estimated pumping speed of 17,000 l/s on air. The facility is also equipped with cryogenic pumps with an estimated pumping speed of 90,000 l/s on Xe.

Facility background pressure was measured with an INFICON Bayard-Alpert Pirani Combination Gauge, model BPG400, calibrated for xenon. This gauge was located at a flange on the side of the test facility approximately 2/3 of a meter downstream from the thruster exit. The indicated pressure was significantly lower when the thruster was running on iodine than when it was running on xenon at nearly identical conditions. However, the gauge responds differently to Xe, I, and I_2 and the correct mix is not known

For an individual gas, the actual pressure is the product of the indicated pressure, p_{ind}, and a calibration factor, C_g. The BPG400 manual identifies calibration factors for Xe and Kr, but not for I or I_2. The relative sensitivity, R_g, is the inverse of the calibration factor. If a hot ionization gauge has not been calibrated for a particular gas, the relative sensitivity may be estimated from electron impact ionization cross sections at 150 eV, e.g. $R_g \approx \sigma_g / \sigma_{N2}$.[22] Table 3 identifies ionization cross sections for N_2, Kr, Xe, I and I_2 from the literature[23,24,25,26] and the corresponding relative sensitivities with respect to N_2 and Xe. The estimated relative sensitivities for I and I_2 with respect to Xe are 1.08 and 1.94, respectively, corresponding to calibration factors of 0.93 and 0.52. Thus, the indicated pressure (which is calibrated for Xe) provides a very conservative estimate of the actual pressure in the facility. The estimated relative sensitivities for Kr and Xe are consistent with calibration factors in the BPG4000 manual. The estimated sensitivities for Kr, Xe, and I_2 are also consistent with empirical sensitivity factors collected by R. Summers at NASA Lewis Research Center.[27]

Table 3 Calculating the Gas Correction Factor[3]

Gas	Ionization Cross Section at 150 eV (Ang^2)	Calculated Relative Sensitivity w.r.t. Xe	Calculated Relative Sensitivity w.r.t. N_2	Reported Relative Sensitivity w.r.t. N_2
N_2	1.75	0.40	1.00	
Kr	3.28	0.75	1.87	1.7 - 1.9
Xe	4.38	1.00	2.50	2.2 - 2.9
I	4.74	1.08	2.71	
I_2	8.48	1.94	4.85	5.4

E. Diagnostics

Plume density was measured with a nude Faraday probe originally developed at MIT which has been cross-calibrated against a larger and well-characterized JPL probe.[28, 29] The Faraday probe was mounted on an automated rotating arm positioned such that the probe swept a 180 degree arc about the center of the exit plane of the thruster, bisecting the plume. The pivot axis was located below the channel exit, and the radial distance from the probe tip to the thruster exit was approximately 37 cm.

The ExB, ESA, and combined probes were sourced from Plasma Controls LLC.[30] These probes were also mounted upon the rotating stage. The ExB probe makes use of the Lorentz force to analyze the ion population by species. However, this measurement includes ions of all energies. The ESA probe uses electrostatic forces to analyze the ion population by charge to mass ratio, but it does not differentiate between species. The combined ESA/ExB probe is able to analyze the ion population by species at a selected energy band. The combination of measurements provides a detailed view of the ion energy distribution.

Thrust was measured using a calibrated thrust stand of the inverted pendulum type.[31] However, some internal degradation of the anode was observed during testing, creating uncertainty as to whether performance changes were related to beam composition or to non-uniformities in the gas flow distribution. Thus, thrust data are not reported.

[3] The ionization cross section for I_2 (8.48 Ang^2) is a theoretical value, and the cross section for I calculated by the same authors using the same methods is 4.17 Ang^2, which is significantly smaller than the reported experimental value of 4.74 Ang^2.

III. Measurements

A Faraday probe was initially used to scope out the plume current profile. Then the ExB probe was used to obtain an overview of the xenon and iodine species present across the whole plume at multiple operating conditions. Next, the ESA probe was used to obtain ion energy distributions at selected operating conditions. Finally, the combined ESA/ExB probe was used to determine current, mass and number distributions (f , g , and h) within the high energy populations of the overall ion energy distribution.

A. Faraday Probe Data

At the beginning of testing, the beam current profile at several conditions was measured with xenon. The probe was swept at r = 37 cm, with the radial axis centered roughly underneath the thruster exit. The angular increment was 5 degrees, and an offset of approximately 2 degrees was corrected during analysis. The probe area was corrected per the method of Brown and Gallimore.[32] The indicated background pressure was $2.6\text{x}10^{-5}$ torr when the facility was evacuated with a diffusion pump. The indicated pressure dropped to $3.6\text{x}10^{-6}$ torr with the addition of cryogenic pumps. This had a marked effect upon the measured current density profile, particularly in the wings. In Fig. 7 the current density at V_d =250 V and P_d =200 W with cryo-pumps operational (which is roughly representative of iodine) is normalized by the value at the center of the beam and multiplied by the weighting factors for current and thrust, $\sin(\theta)$ and $\sin(\theta)\cos(\theta)$. The plot of $j(\theta)\sin(\theta)\cos(\theta)$ shows that the axial momentum is almost entirely within 45 degrees of the centroid, but peaks at 12 degrees - not at the center. Viewing this as a histogram, approximately 18% of the thrust is centered around 12 degrees, 16% is centered around 17 degrees, and so on. Most of the momentum is found from 10 degrees outward – a region where significant iodine dimer populations are sometimes observed.

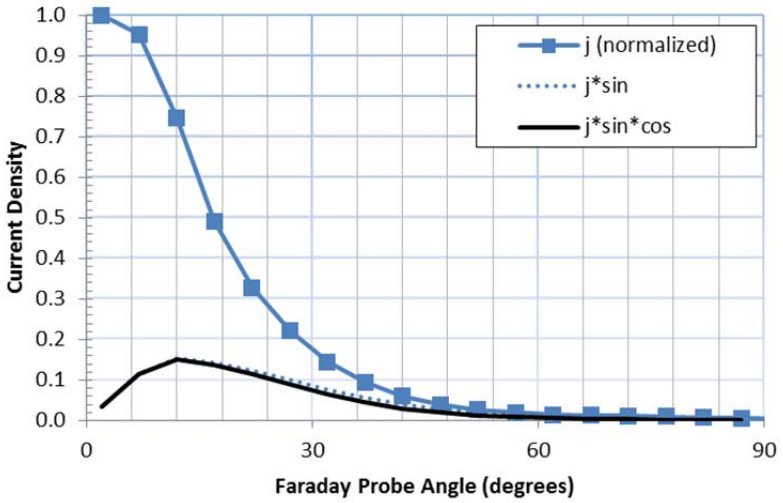

Fig. 7 Current density profile for thruster flowing Xe with weighting factors

B. ExB Probe Data

The ExB probe was used to obtain an overview of the species present in the plume as a function of θ, V_d, and I_d. Sample ExB data for iodine at V_d =250 V and P_d =150 W (I_d =0.6 A) are plotted in Fig. 8 for $\theta \leq 50^{o}$. This condition was selected to show for its relatively large dimer population, seen here at approximately 15 volts. From left to right, the signals represent I_2^+, I^+, I^{2+} and I^{3+}. Xenon ExB data at the same conditions are plotted in Fig. 9. From left to right, the signals represent Xe^+, Xe^{2+}, and Xe^{3+}.

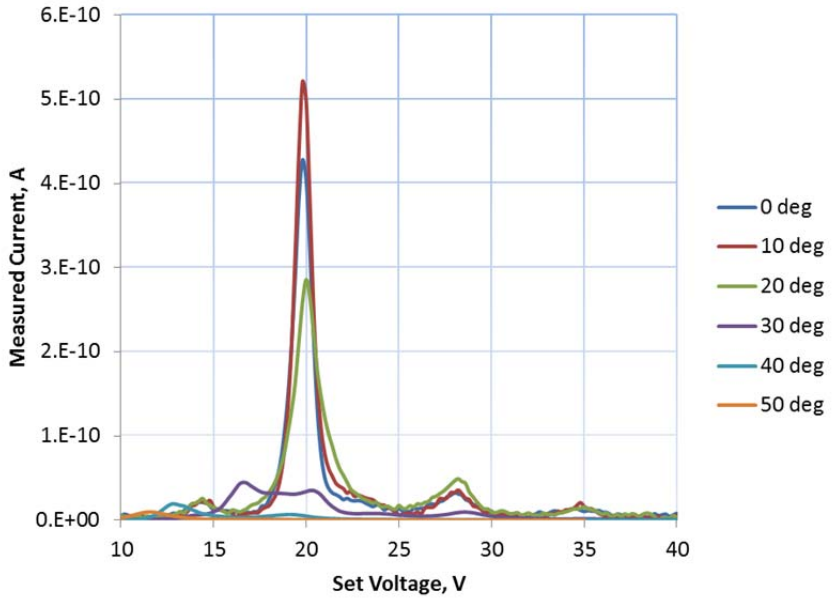

Fig. 8 Iodine ExB plume sweep at 250V 150W ($p_{ind} \approx 4.5\text{x}10^{-6}$ torr)

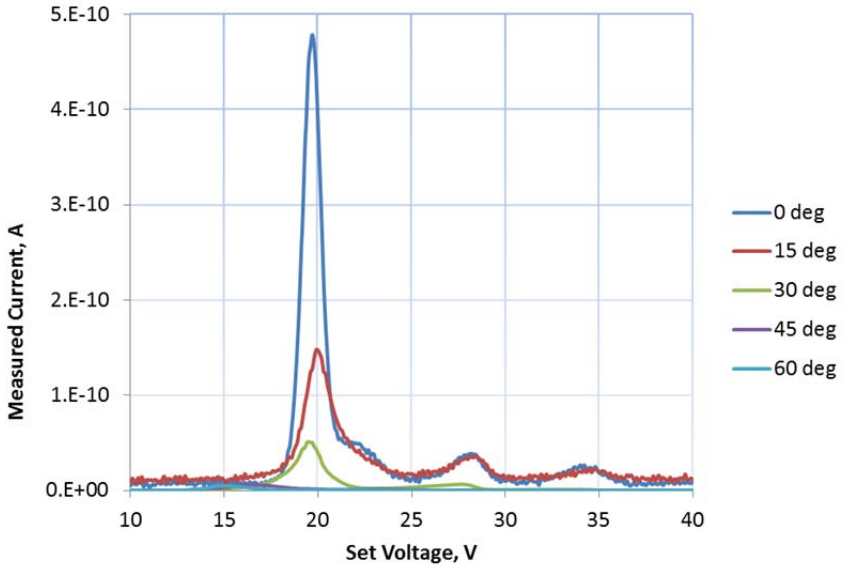

Fig. 9 Xenon ExB plume sweep at 250V 150W ($p_{ind} \approx 2\text{x}10^{-5}$ torr)

The size of each population was determined by the area under the curve. For each population, area A was taken to be the height of the peak multiplied by the width at half maximum. The base from which the height was measured was determined by averaging the low energy portion of the data (where no populations exist). The parameter f is the fraction of the total collected current by species. This was calculated as

$$f_k = \frac{A_k}{\sum_k A_k}. \tag{15}$$

For iodine, the four assumed species were I_2^+, I^+, I^{2+}, and I^{3+}. For xenon, the species were Xe^+, Xe^{2+}, and Xe^{3+}.

At $\theta \leq 20^{o}$, ExB measurements indicate f associated with I_2^+ varies between 0% and 6%. The largest fractions were measured at low discharge current (I_d =0.6 A). Much larger I_2^+ fractions were measured at $\theta \geq 30^{o}$. However, ESA measurements described in the next section showed that low energy ions are a significant fraction of the total beginning at $\theta \geq 15^{o}$. To determine the potential effect of dimers upon performance, the low energy portion of the distribution must be filtered out. This is accomplished with the combined probe.

C. ESA Probe

The ESA probe was used to determine the ion energy distribution as a function of θ for each thruster operating point (V_d , P_d) of interest. Fig. 10 shows the iodine ESA sweep at V_d =250 V and P_d =150 W (I_d =0.6 A) . Fig. 11 shows the xenon ESA sweep at the same discharge conditions, but higher background pressure. For each such set of sweeps at a given operating condition, the significant ion populations were identified. Near the beam centroid, most of the ions were highly energetic. Lower energy populations increased with θ in relative magnitude. At $\theta \geq$ 15, the velocity distribution is far from Maxwellian.

D. Combined Probe

The combined ESA/ExB probe was used to analyze specific populations selected from the ESA data. The current fractions f_k were determined from areas as before. Number fractions, h_k , were determined by dividing the collected current associated with each species by the charge associated with that species:

$$h_k = \frac{A_k / q_k}{\sum_k A_k / q_k} . \tag{16}$$

Mass fractions, g_k , were determined by multiplying the current associated with each species by mass, and dividing by charge:

$$g_k = \frac{A_k M_k / q_k}{\sum_k A_k M_k / q_k} . \tag{17}$$

For xenon, h and g are equivalent.

Iodine ESA/ExB data for V_d =250 V and P_d =150 W (I_d =0.6 A) are shown in Fig. 12. Sweeps were taken at the primary energy peak at 217V for all angles. The indicated tank pressure was 6.6×10^{-6} torr, and the actual pressure was lower by a factor of 0.52 or greater. By current, the measured high energy dimer fraction at the beam centroid was 2.2% ($f_k \approx 0.022$). By number and mass, the fractions at θ =0 were 2.3% ($h_k \approx 0.023$) and 4.5%, (g_k =0.045). Much higher fractions were measured at larger angles. For instance, at θ =30 degrees, the dimer fraction by mass was 22% ($g_k > 0.20$).

Xenon data for V_d =250 V and P_d =150 W (I_d =0.6 A) are shown in Fig. 13 and summarized in Table 5. Sweeps at 250 V, 150 W were taken at primary energy peaks of 215V or 220 V. The indicated background pressure was $2.4 \times 10^{-}$torr. By current, the high energy Xe^{2+} fraction was 22% ($f_k = 0.22$) at θ =30 degrees. By number and mass, Xe^{2+} was 13% of the high energy plume ($h_k = g_k = 0.13$) at this same location.

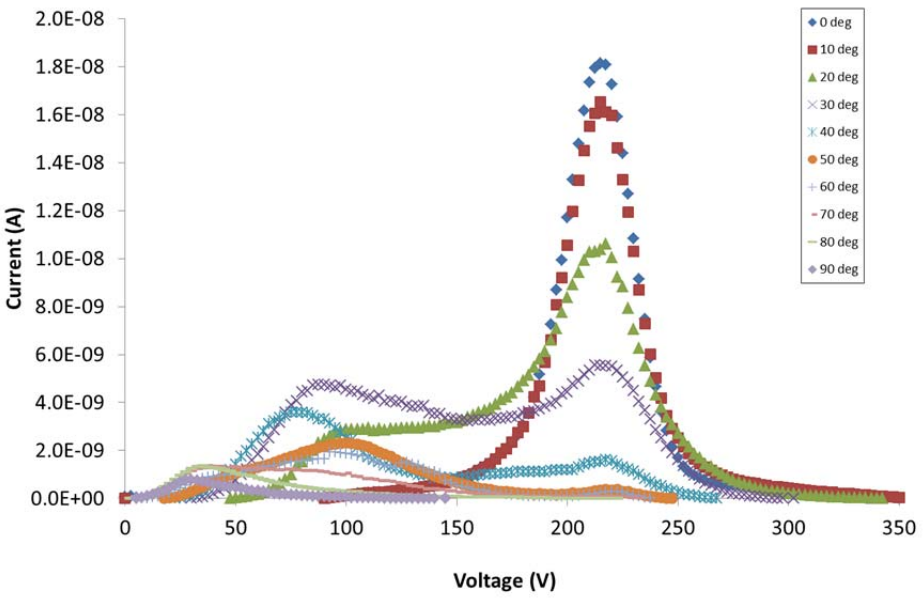

Fig. 10 ESA sweep of Iodine plume at 250V 150W (p_{ind} ≈ 5.4x10^{-6} torr)

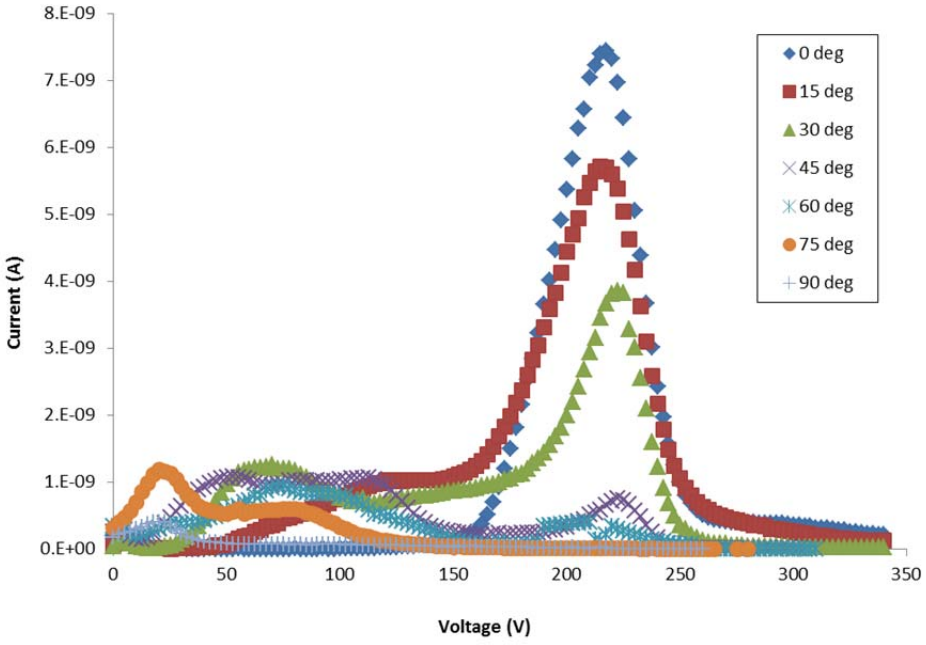

Fig. 11 ESA sweep of xenon plume at 250V 150W (p_{ind} ≈ 1x10^{-5} torr)

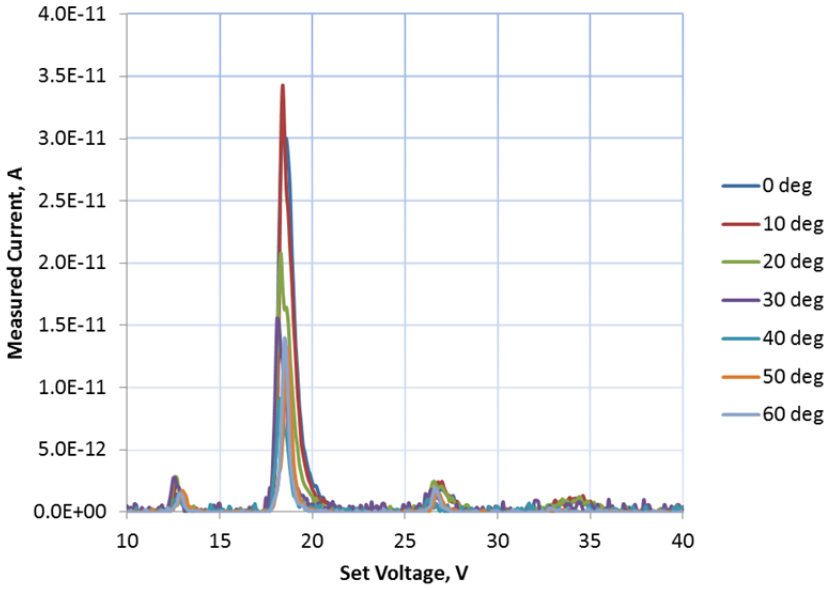

Fig. 12 Iodine combined ESA/ExB plume sweeps taken at 250 V, 150 W ($p_{ind} \approx 6.6\text{x}10^{-6}$ torr)

Table 4. Iodine ESA/ExB distributions at 250 V, 150 W

Angle (deg)	Species	Mass	Charge	f	g	h
0	I_2^+	2	1	0.02	0.04	0.02
0	I^+	1	1	0.92	0.93	0.95
0	I^{2+}	1	2	0.05	0.03	0.03
0	I^{3+}	1	3	0.00	0.00	0.00
10	I_2^+	2	1	0.04	0.08	0.04
10	I^+	1	1	0.86	0.87	0.91
10	I^{2+}	1	2	0.09	0.05	0.05
10	I^{3+}	1	3	0.01	0.00	0.00
20	I_2^+	2	1	0.07	0.14	0.07
20	I^+	1	1	0.80	0.80	0.86
20	I^{2+}	1	2	0.13	0.07	0.07
20	I^{3+}	1	3	0.00	0.00	0.00
30	I_2^+	2	1	0.12	0.22	0.12
30	I^+	1	1	0.76	0.72	0.81
30	I^{2+}	1	2	0.12	0.06	0.06
30	I^{3+}	1	3	0.00	0.00	0.00
40	I_2^+	2	1	0.10	0.18	0.10
40	I^+	1	1	0.85	0.80	0.87
40	I^{2+}	1	2	0.05	0.02	0.03
50	I_2^+	2	1	0.11	0.20	0.11
50	I^+	1	1	0.79	0.75	0.83
50	I^{2+}	1	2	0.11	0.05	0.06
60	I_2^+	2	1	0.08	0.17	0.09
60	I^+	1	1	0.80	0.78	0.85
60	I^{2+}	1	2	0.12	0.06	0.06
70	I_2^+	2	1	0.00	0.00	0.00
70	I^+	1	1	0.91	0.95	0.95
70	I^{2+}	1	2	0.09	0.05	0.05

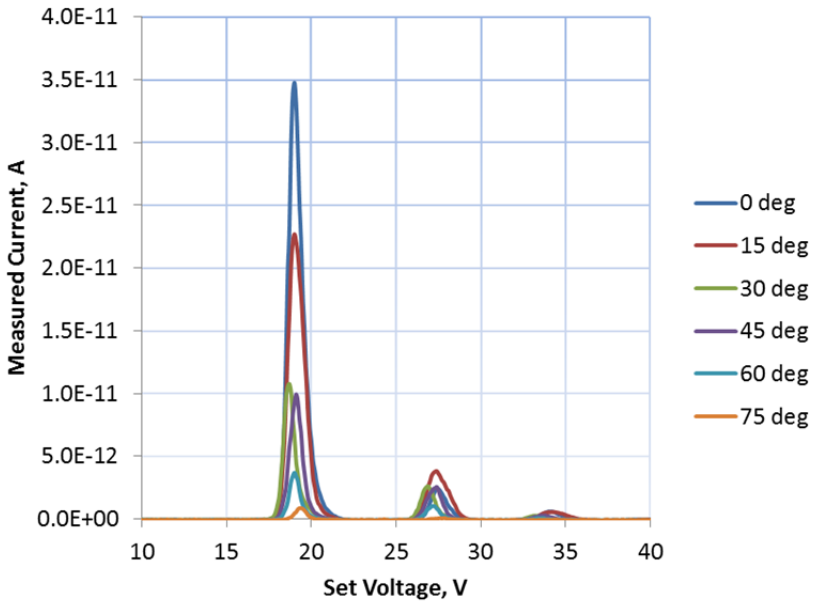

Fig. 13 Xenon combined ESA/ExB plume sweeps taken at 250 V, 150 W

Table 5 Xe ESA/ExB Data at 250 V, 150 W

Angle (deg)	Species	Mass	Charge	f	h=g
0	Xe^{+}	1	1	0.89	0.95
0	Xe^{2+}	1	2	0.08	0.04
0	Xe^{3+}	1	3	0.03	0.01
15	Xe^{+}	1	1	0.79	0.89
15	Xe^{2+}	1	2	0.17	0.10
15	Xe^{3+}	1	3	0.04	0.01
30	Xe^{+}	1	1	0.75	0.86
30	Xe^{2+}	1	2	0.22	0.13
30	Xe^{3+}	1	3	0.03	0.01
45	Xe^{+}	1	1	0.72	0.85
45	Xe^{2+}	1	2	0.24	0.14
45	Xe^{3+}	1	3	0.04	0.01
60	Xe^{+}	1	1	0.71	0.84
60	Xe^{2+}	1	2	0.26	0.15
60	Xe^{3+}	1	3	0.03	0.01
75	Xe^{+}	1	1	0.82	0.90
75	Xe^{2+}	1	2	0.18	0.10

IV. Discussion

The influence of multiple species upon the overall efficiency and thrust to power can be quantified using the molar (number) fraction of the flux, Γ. Locally, the momentum flux is proportional to $\sum_k h_k M_k v_k$, where $v_k = \sqrt{2q_k V / M_k}$. The local mass flux is proportional to $\sum_k h_k M_k$. If $I_d = I_c \propto I_b$, the energy cost of the ions at constant voltage may be assumed to vary in proportion to the ion current density and, this, in proportion to $\sum_k h_k q_k$. (In actuality, with each of the k species, there may be a wide variation in point of origin). With these assumptions, in analogy to equation (7), a species efficiency, η_s, may be written:

$$\eta_s \propto \frac{(\sum_k h_k M_k v_k)^2}{\sum_k h_k M_k \sum_k h_k q_k}. \tag{13}$$

In a similar fashion, a thrust to power factor may be written:

$$\frac{T}{P} \propto \frac{\sum_k h_k M_k v_k}{\sum_k h_k q_k}. \tag{14}$$

For the three primary ionic species in the beam, normalized values of charge, mass, velocity, momentum, and energy are shown in Table 6. Although I^{2+} is twice as energetic as I and I_2^+, each I^{2+} ion contributes two electrons to the discharge instead of one. I^{2+} is $\sqrt{2}$ times as fast as I^+ and twice as fast as I_2^+, but I_2^+ and I^{2+} have the same momentum. With these values, relative values of η_s and T/P can be estimated from equations 13 and 14 as h_1, h_2, and h_3 are varied.

Table 6 Iodine Species and their Relative Properties

Parameter	Symbol	I^+	I^{2+}	I_2^+
Charge	q	1	2	1
Mass	M	1	1	2
Charge/Mass	q/M	1	2	0.5
Energy	ε	1	2	1
Velocity	v	1	1.41	0.71
Momentum	p	1	1.41	1.41
Momentum/Energy	p/ε	1	0.71	1.41

Fig. 14 plots Equation 13 as a function of the singly charged dimer (I_2^+) and monomer (I^+), fractions, assuming the rest of the discharge is comprised of doubly charged monomers (I^{2+}). The curves represent I^+ fractions. The X-axis is the I_2^+ fraction. The presence of multiple species always exacts an efficiency loss. However, η_s is always greater than 93% when more than 50% of the beam is I^+. This result also is significant for its relation to two thrusters operating next to each other at different specific impulse, or a multiple channel "nested" Hall thruster where the two channels operate at specific impulse; a modest difference in specific impulse has only a minor impact upon efficiency.

Fig. 15 plots the net thrust to power (equation 14) as function of the I_2^+ and I^+ fractions, again assuming the rest of the discharge is comprised of I^{2+}. This figure shows that I_2^+ could increase p/ε significantly.

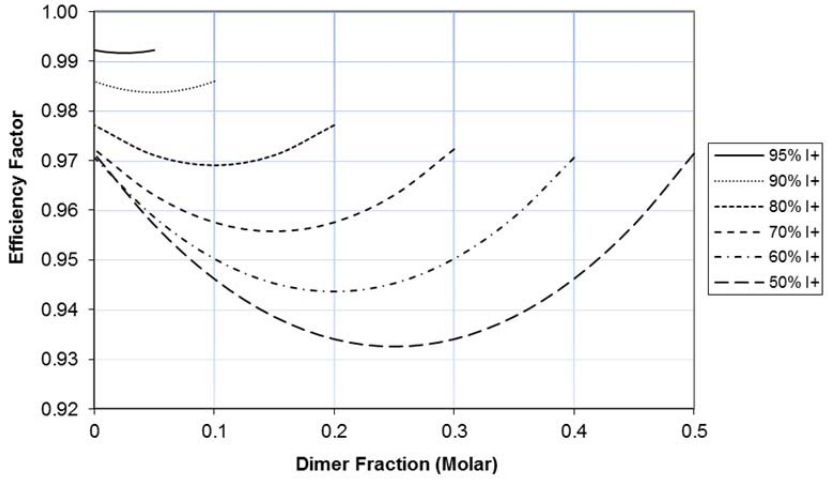

Fig. 14 Efficiency Factor as a Function of Molar (Number) Fractions

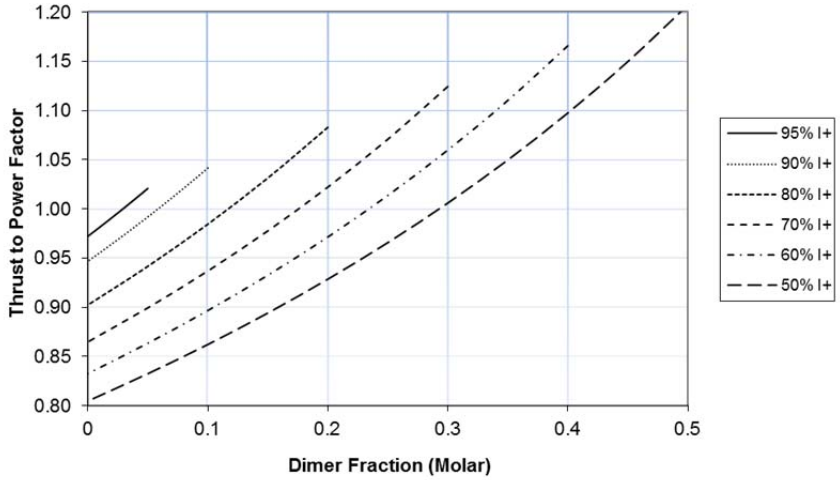

Fig. 15 Thrust to Power Factor as a Function of Molar (Number) Fractions

The following example helps clarify the meaning of the plots. If the flux is 50% I^+ ($h_1 = 0.5$) , the plots assume $h_2 + h_3 = 0.5$. The worst case for efficiency occurs when $h_2 = h_3$ (equal molar fractions of I_2^+ and I^{2+}), at which η_s = 0.933 (Fig. 14) and p/ε =0.966 (Fig. 15). The best case for efficiency occurs when $h_2 = 0$ or $h_3 = 0$, in which case η_s = 0.971. In this best case, if there is no I^{2+}, then p/ε =1.21. If there is no I_2^+, then p/ε =0.805.

The ExB probe measurements showed the presence of molecular species throughout the central, momentum carrying portion of the plume. However, the dimer population varied with operating conditions and seemed to be concentrated off axis. Table 7 summarizes the ESA/ExB current fractions, f , across a broad range of operating conditions. These data seem to indicate that the dimer fraction is largest when the current is low and the discharge is rarified. The highest dimer fractions by current are observed at 250 V and 150 W, where I=0.6 A. Relatively large, localized populations were also found at I_d =0.71 and I_d =0.8 A.

Table 7 Summary of iodine ESA/ExB Probe Current Fractions at High Energy Peaks

		Discharge Conditions							
		150	200	250	250	300	350	350	[V]
Angle [deg]	Species	1.00	1.00	0.60	0.80	0.80	0.71	1.00	[A]
		150	200	150	200	240	250	350	[W]
0	I_2^+			0.02	0.01		0.01		
0	I^+	0.53	1.00	0.92	0.95	0.93	0.94	0.96	
0	I^{2+}	0.47	0.00	0.05	0.04	0.07	0.05	0.04	
0	I^{3+}			0.00	0.00	0.00			
10	I_2^+			0.04	0.03	0.02	0.02		
10	I^+	0.98	0.83	0.86	0.82	0.83	0.90	0.88	
10	I^{2+}	0.02	0.14	0.09	0.08	0.11	0.08	0.12	
10	I^{3+}		0.03	0.01	0.07	0.05			
20	I_2^+			0.07	0.02	0.02	0.06	0.00	
20	I^+	0.99	0.40	0.80	0.85	0.82	0.77	0.86	
20	I^{2+}	0.01	0.60	0.13	0.13	0.15	0.18	0.13	
20	I^{3+}			0.00	0.01	0.00			
30	I_2^+			0.12	0.00	0.03		0.02	
30	I^+	1.00	0.85	0.76	0.95	0.77	0.86	0.79	
30	I^{2+}		0.15	0.12	0.00	0.18	0.14	0.19	
30	I^{3+}			0.00	0.05	0.03			
40	I_2^+			0.10	0.00	0.05	0.01	0.02	
40	I^+	1.00	0.85	0.85	0.90	0.76	0.87	0.75	
40	I^{2+}		0.15	0.05	0.10	0.19	0.13	0.23	
50	I_2^+			0.11	0.00	0.04	0.01	0.00	
50	I^+	1.00	1.00	0.79	0.91	0.82	0.90	0.84	
50	I^{2+}			0.11	0.09	0.14	0.09	0.16	
60	I_2^+			0.08	0.06	0.04	0.08	0.00	
60	I^+		1.00	0.80	0.81	0.92	0.81	0.83	
60	I^{2+}			0.12	0.13	0.04	0.12	0.17	
70	I_2^+			0.00		0.04			
70	I^+		1.00	0.91		0.95	1.00	0.81	
70	I^{2+}			0.09		0.00		0.19	

Fig. 16 plots the mass fraction, g_k, measured verses angle for the 250 V, 150 W conditions. The high energy dimer fraction is smaller near the beam centroid than off axis. The measured I_2^+ fraction is greatest from 30 to 50 degrees, which is the peak of the weighting function for thrust given in equation 11. Dimers are also present in the far field (50-60 degrees), but these diminish in significance due to the exponential decrease in current density compounded by the as the weighting factor $\cos(\theta)\sin(\theta)$.

The measurements indicate that the dimer fraction at some conditions is sufficient to increase thrust to power by a small, but measurable amount. Per Table 4, at 250 V, 150 W the data show a dimer number fraction between 2 and 12 percent in the central part of the plume. Therefore, per Fig. 14 the species or poydispersivity efficiency is likely to be 98 to 99% and the thrust to power factor, p/ε will be between 0.95 and 1.05, depending on the detailed distribution of momentum vs. angle.

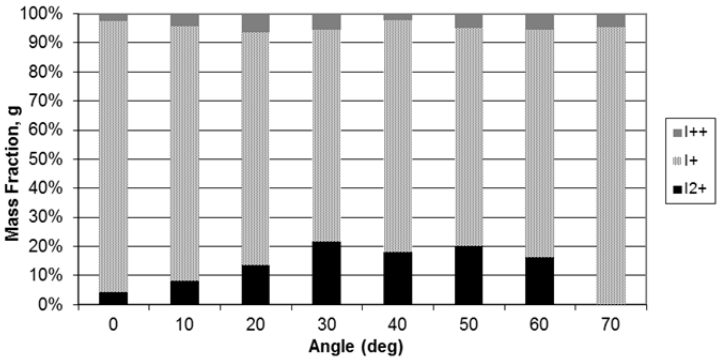

Fig. 16 Mass fraction of flux at 250 V, 150 W

This method used to determine f is similar to the "method of triangle fitting" recommended by Shastry et al. and suggested by Beal.[33,34] However, Shastry recommends multiplying the peak height by the half width at half maximum, where the half width is defined on the high energy side of the curve. The analysis here uses the full width. To determine the sensitivity of the results to this difference, a subset of the iodine data at 250 V, 150 W were re-analyzed using both methods. In relative terms, using the half width on the high side decreased the dimer current fractions by 9, 12, and 20% at 20, 30, and 40 degrees, respectively. In absolute terms, the difference was 0.5, 1.4 and 1.7%. Shastry also recommends the use of a charge exchange correction model. No such correction was applied to the data because the composition of the background gas is unclear.

V. Conclusions

Prior performance measurements showed that iodine could be an attractive replacement for xenon in Hall effect thrusters. Overall performance was found to be on par with xenon, while initial plume measurements showed a well collimated beam profile and a small but significant population of ionized dimers. At some conditions, higher thrust to power was measured with iodine than with xenon.

The data reported here lend further insight into the plume structure and ion species distribution. Significant populations of diatomic iodine were observed in the plume. These dimers were concentrated slightly off axis from the thruster centroid, and were observed to vary with thruster operating conditions. Such dimers could change the observed thruster efficiency and thrust to power by measurable amounts. In any case, dimers should be accounted for in future analytical and numerical studies of iodine fueled thrusters.

Acknowledgments

The authors wish to acknowledge the Air Force Research Laboratory (AFRL) for support under contract FA9300-10-C-2108.

References

[1] Janes, G., Dotson, J, and Wilson, T., "Momentum Transfer Through Magnetic Fields," *Proceedings of Third Symposium on Advanced Propulsion Concepts, Vol. 1*, Cincinnati, OH, October 2-4 1962, pp. 153-175

[2] Meyerand, R., G., "Momentum Transfer Through the Electric Fields," *Proceedings of Third Symposium on Advanced Propulsion Concepts, Vol. 1*, Cincinnati, OH, 2-4 October, 1962, pp. 177-190.

[3] Seikel, G. R., "Generation of Thrust – Electromagnetic Thrusters," *Proceedings of the NASA-University Conference on the Science and Technology of Space Exploration*, Vol. 2, Nov. 1962, pp. 171-176.

[4] Morozov, A., I., "The Conceptual Development of Stationary Plasma Thrusters," *Plasma Physics Reports*, Vol. 29, No. 3, 2003, pp. 235-250.

[5] Hruby, V., Monheiser, J., Pote, B., Freeman, C., and Connolly, W., "Low Power, Hall Thruster Propulsion System," *26th International Electric Propulsion Conference*, IEPC paper 99-092, Kitakyushu, Japan, Oct 99.

[6] Szabo, J., Pote, B., Paintal, S., Robin, M., Hillier, A., Branam, R., Huffman, R., "Performance Evaluation of an Iodine Vapor Hall Thruster", *AIAA Journal of Propulsion and Power*, Vol. 28, No. 4, July/August 2012, pp. 848-857. doi: 10.2514/1.B34291

[7] Hillier, A., "Revolutioning Space Propulsion Through the Characterization of Iodine as Fuel for Hall-Effect Thrusters," M.S. Thesis, Air Force Institute of Technology, Wright-Patterson Air Force Base, Ohio, 2011.
[8] Szabo, J., Robin, M., Paintal, Pote, B., S., Hruby, V., "High Density Hall Thruster Propellant Investigations," *48th AIAA/ASME/SAE/ASEE Joint Propulsion Conference,* AIAA Paper 2012-3853, July 2012.
[9] Hruby, V., Monheiser, J., Pote, B., "Tandem Hall Field Plasma Accelerator," United States Patent 6,150,764, 21 Nov 2000.
[10] Janes, G., Lowder, R., "Anomalous Electron Diffusion and Ion Acceleration in a Low-Density Plasma," *The Physics of Fluids*, Vol. 9., No. 6, June 1966, pp. 1115-1123.
[11] Joshipura, K. N., Limbachiya, C. G, "Theoretical total ionization cross-sections for electron impact on atomic and molecular halogens," *International Journal of Mass Spectrometry*, 216 (2002), pp. 239-247.
[12] *CRC Handbook of Chemistry and Physics*, 83rd Edition, CRC Press LLC, 2002.
[13] Syage, J., "Electron-impact cross sections for multiple ionization of Kr and Xe," *Phys. Rev. A*, 46, 9, 1992, pp. 5666-5679.
[14] Hayes, T., Wetzel, R., Freund, R., "Absolute electron-impact-ionization cross-section measurements of the halogen atoms," *Physical Review A*, 35, 2, January 15, 1987, pp, 578-584.
[15] Ali, M., and Kim, Y., "Ionization cross sections by electron impact on halogen atoms, diatomic halogen and hydrogen halide molecules," *J. Phys. B: At. Mol. Opt. Phys.* 41 (2008), 145202.
[16] Szabo, J., Martinez-Sanchez, M., Monheiser, J., "Application of 2-D Hybrid PIC Code to Alternative Hall Thruster Geometries," *34th AIAA/ASME/ASE/ASEE Joint Propulsion Conference*, AIAA Paper 98-3795, Cleveland, OH, July 98.
[17] Parra, F., Ahedo, E., Fife, J., Martinez-Sanchez, M., *J. Appl. Phys.*, 100, 023304 (2006).
[18] Szabo, J. "Fully Kinetic Numerical Modeling of a Plasma Thruster," Ph.D. Thesis, Department of Aeronautics and Astronautics, Massachusetts Institute of Technology, Cambridge, MA, 2001.
[19] Goebel, D., Katz, I., "*Fundamentals of Electric Propulsion: Ion and Hall Thrusters*," 1st ed., John Wiley & Sons, Hoboken, NJ, 2008.
[20] Lozano, P., "Studies on the Ion-Droplet Mixed Regime in Colloid Thrusters," Ph.D. Thesis, MIT, 2003.
[21] Brown, D., Larson, C., Beal, B., Gallimore A., "Methodology and Historical Perspective of a Hall Thruster Efficiency Analysis," *Journal of Propulsion and Power*, Vol. 25, No. 6, Nov-Dec 2009.
[22] Stanford Research Systems, "Bayard-Alpert Ionization Gauges," technical note.
[23] Itikawa, Y., "Cross Sections for Electron Collisions with Nitrogen Molecules," J. Phys. Chem. Ref. Data, Vol. 35, No. 1, 2006.
[24] Hayes, T., Wetzel, R., Freund, R., "Absolute electron-impact-ionization cross-section measurements of the halogen atoms," *Physical Review A*, 35, 2, January 15, 1987, pp, 578-584.
[25] Wetzel, R., Baiocchi, F., Hayes, T, Freund, R., "Absolute cross sections for electron-impact ionization of the rare-gas atoms by the fast-neutral-beam method," *Physical Review A*, 35, 2, January 15, 1987, pp, 559-577.
[26] Ali, M., and Kim, Y., "Ionization cross sections by electron impact on halogen atoms, diatomic halogen hydrogen halide molecules," J. Phys. B: At. Mol. Opt. Phys. 41 (2008) 145202.
[27] R. Summers, NASA Lewis Research Center, NASA Technical Note TND-5285, National Aeronautics and. Space Administration, Washington, DC, June 1969
[28] Azziz, Y., "Experimental and Theoretical Characterization of a Hall Thruster Plume," Ph. D. Dissertation, Department of Aeronautics and Astronautics, Massachusetts Institute of Technology, Boston, MA, 2007.
[29] Walker, M., Hofer, R. and Gallimore, A., "The Effects of Nude Faraday Probe Design and Vacuum Facility Backpressure on the Measured Ion Current Density Profile of Hall Thruster Plumes," *38th AIAA/ASME/SAE/ASEE Joint Propulsion Conference*, AIAA Paper 2002-4253, Indianapolis, IN, July 7-10, 2002.
[30] Farnell, C., and Williams, J., "ExB Probe Operating Manual," Colorado State University, Ft. Collins, Instrument Manual 2007.
[31] Haag, T., *Review of Scientific Instruments*, 62, 1186 (1991).
[32] Brown, D., Gallimore, A., "Evaluation of ion collection area in Faraday probes," Review of Scientific Instruments 81, 063504 (2010).
[33] Beal, B., Ph.D. thesis, University of Michigan, 2004.
[34] Shastry, R., Hofer, R., Reid, B., Gallimore, A., "Method for analyzing ExB probe spectra from hall thruster plumes," Review of Scientific Instruments 80, 063501 (2009).